Applied Surface Science 387 (2016) 51–57

Contents lists available at ScienceDirect

Applied Surface Science

journal homepage: www.elsevier.com/locate/apsusc

VO_x effectively doping CVD-graphene for transparent conductive films

Qinghua Ji[a], Liangjing Shi[a], Qinghong Zhang[b], Weiqi Wang[a], Huifeng Zheng[a], Yuzhi Zhang[c], Yangqiao Liu[a,*], Jing Sun[a,*]

[a] State Key Laboratory of High Performance Ceramics and Superfine Microstructure, Shanghai Institute of Ceramics, Chinese Academy of Sciences, 1295 Dingxi Road, Shanghai 200050, China
[b] State Key Laboratory of Modification of Chemical Fibers and Polymer Materials, College of Material Science and Engineering, Donghua University, 2999 North Renmin Road, Shanghai 201620, China
[c] The Key Laboratory of Inorganic Coating Materials, Shanghai Institute of Ceramics, Chinese Academy of Sciences,1295 Dingxi Road, Shanghai 200050, China

ARTICLE INFO

Article history:
Received 6 March 2016
Received in revised form 16 May 2016
Accepted 15 June 2016
Available online 17 June 2016

Keywords:
CVD graphene
VO_x doping
Stability
Optical properties
Doping mechanism

ABSTRACT

Chemical vapor deposition(CVD)-synthesized graphene is potentially an alternative for tin-doped indium oxide (ITO) transparent conductive films (TCFs), however its sheet resistance is still too high to meet many demands. Vanadium oxide has been widely applied as smart window materials, however, no study has been reported to use it as dopant to improve the conductivity of graphene TCFs. In this study, we firstly reported that VO_x doping can effectively lower the sheet resistance of CVD-graphene films while keeping its good optical properties, whose transmittance is as high as 86–90%. The optimized VO_x-doped graphene exhibits a sheet resistance as low as 176 Ω/□, which decreases by 56% compared to the undoped graphene films. The doping process is convenient, stable, economical and easy to operate. What is more, VO_x can effectively increase the work function(WF) of the film, making it more appropriate for use in solar cells. The evolution of the VO_x species annealed at different temperatures below 400 °C has been detailed studied for the first time, based on which the doping mechanism is proposed. The prepared VO_x doped graphene is expected to be a promising candidate for transparent conductive film purposes.

1. Introduction

Transparent conductive films (TCFs), which possess both high electrical conductivity and high optical transmittance, are widely used in industry, especially in information (displays) and solar cell architecture (window glass) [1–3]. Up to now, tin-doped indium oxide (In_2O_3:Sn, abbreviated ITO) has been the most commonly used TCFs material [1]. However, ITO has some drawbacks such as its instability in the presence of acid or base, limited transparency in the near-infrared region and the lack of flexibility, as well as its increasing price due to the rareness of the indium element on earth [4]. Despite of the great potential of chemical vapor deposition(CVD) synthesized graphene to substitute for ITO TCFs in the future [5], its sheet resistance is still too high to replace ITO films, especially in fields demanding low sheet resistance, such as solar cells. For instance, with the same transparency of 85% at 550 nm, graphene films usually exhibit sheet resistances in the range of 100–500 Ω/□, about several times higher than that of ITO counterparts. What's more, the work function (WF) of graphene TCFs needs to be adjusted to match with the energy levels of semiconductor layers for decreasing the energy loss in solar cells. The WF of undoped graphene is around 4.5 eV [6], however, it is more desirable to be increased to above 5 eV as the cathode material to match with the HOMO levels of most organic acceptors for accelerating the carrier injections. Therefore, graphene needs to be modified from both the sheet resistance and the WF aspects for implementing photovoltaic purposes.

Doping is considered as a promising route to improve the carrier concentration and therefore improve the electrical conductivity. Due to the p-type semiconductor nature of graphene under ambient condition on the SiO_2 [7], p-type dopants are more effective in decreasing its sheet resistance by introducing more hole carriers [2]. There are many p-type dopants that have been discovered to lower the sheet resistance of graphene and modify its WF, such as organic molecules (TFSA [8], DDQ [9], F4-TCNQ [10]), inorganic salt/acid (HNO_3 [11], $AuCl_3$ [12,13], $SOCl_2$ [14]), metal particles [1,2,15,16] and metal oxide [17]. However, organic molecules are generally unstable in the ambient air, while, $AuCl_3$ is too expensive as dopants. In contrast, metal oxide draws much more attention in recent years due to its low price, efficient doping effect and higher stability. Typically, molybdenum oxide (MoO_3) was reported to effectively dope graphene, by which the sheet resistance of the

* Corresponding authors.
E-mail addresses: yqliu@mail.sic.ac.cn (Y. Liu), jingsun@mail.sic.ac.cn (J. Sun).

http://dx.doi.org/10.1016/j.apsusc.2016.06.086
0169-4332/

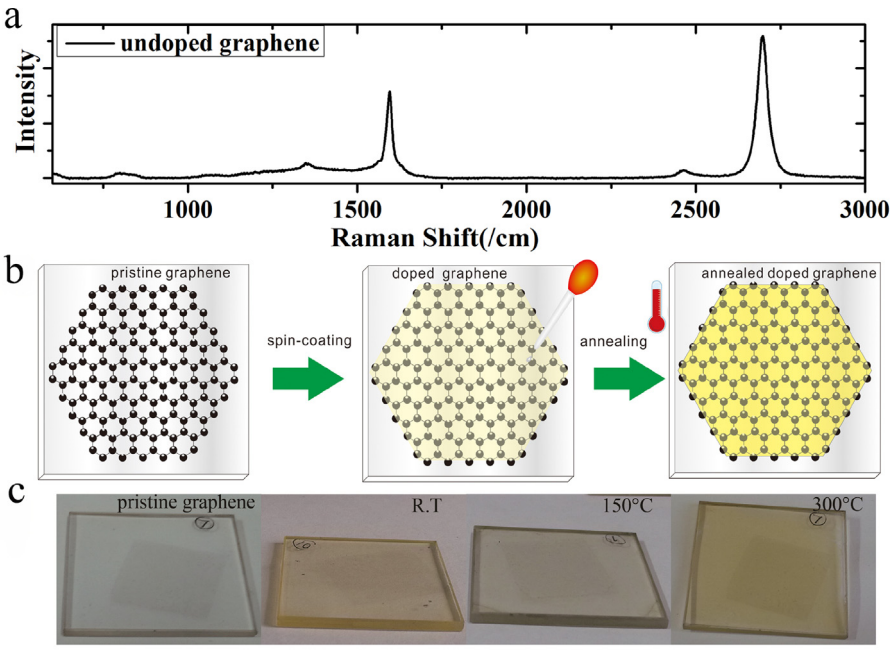

Fig. 1. (a) Raman spectra of the undoped graphene. (b) Flowchart of the experimental procedure and (c) photographs of undoped graphene, doped graphene annealed at room temperature (RT), 150 °C and 300 °C, respectively, from left to right.

graphene decreased from 465 Ω/□ to 270 Ω/□ [17]. However, the thermal evaporation method they adopted is severe in vacuum degree and complicated in operation, as well as an annealing atmosphere of Ar, which increases the cost. Vanadium oxide (VO_x) is a well-known high work-function material and has been commonly used as an effective hole extraction layer within organic photovoltaic devices [18,19]. Therefore, it is expected that holes will be injected from VO_x to semiconductors with lower work function, i.e., a p-type doping of the semiconductor is expected to occur. Furthermore, it can be easily deposited with cheap solvent-based methods, such as sol–gel method, etc [20,21]. All these properties make VO_x an effective doping candidate for graphene.

In the present study, we reported the successful doping of graphene by VO_x for the first time. A significant reduction in sheet resistance as well as an effective increment of the WF was observed. Doping conditions, especially thermal treatment temperatures, were optimized for obtaining the utmost doping effect. The finding may offer an effective way to turning the properties of the graphene TCFs for transparent conductive films purposes.

2. Experimental details

2.1. The preparation of graphene

Graphene samples were grown on 2 cm × 2 cm copper foil (99.8% Alfa) with a thickness of 25 μm in the quartz tube furnace system using ambient pressure chemical vapor deposition (APCVD) method. The copper foil was pretreated at 1000 °C for 30 min with H_2 in the quartz tube at a flow rate of 100 sccm. After preheating procedure, the temperature was increased to 1050 °C in 5 min, then a mixture of methane (CH_4), hydrogen (H_2) and argon (Ar) gas was flown into the tube. Six minutes later, the furnace was rapidly cooled down to room temperature in 10 min.

2.2. The transfer of graphene

The copper foil with graphene grown on was deposited a film of poly[methyl methacrylate] (PMMA) by spin coating 46 mg mL^{-1} PMMA solution in chlorobenzene, which was then exposed at room temperature for 5 min. The ammonium persulfate (1 M $(NH_4)_2S_2O_8$) solution was used to etch away the copper foil at room temperature for 12–18 h. After etching, the remaining PMMA-coated graphene was carefully dipped into deionized water to remove any residual etchant. The PMMA-coated graphene sheet was then transferred and tightly adhered onto quartz substrates. Afterwards, PMMA was thoroughly removed by immersion in an acetone bath for 30 min. Finally, the graphene film on quartz substrate was annealed in H_2 for 1 h at 400 °C to remove the remaining PMMA.

2.3. Doping and annealing procedure

The $VO(OC_3H_7)_3$ (purity 99%, Sigma-Aldrich) was diluted with isopropanol at the volume ratio of 1/70. Then, this solution was spin coated onto graphene-on-quartz substrates at 4000 rpm for 30 s. Afterwards, the doped graphene film was annealed at different temperatures in air or Ar atmosphere.

2.4. Characterization of the graphene films

The sheet resistance of the doped graphene was measured by 4-point probe method (Loiesla-Ax Mcp-T370). The optical properties of the VO_x-doped graphene layer were characterized with UV–vis spectroscopy (Lambda 950, Perkin Elmer). X-Ray Diffraction (XRD) (Bruker D8 CEVANCE) was used to characterize the phase evolution of vanadium pentoxide. Field emission scanning electron microscope (FESEM) (SU8220) was used to examine the surface of the p-doped graphene layer. Raman spectroscopy (DXR Raman Microscope) and X-ray photoemission spectroscopy (XPS)(ESCAlab 250) were used to characterize the doping mechanism. Scanning Kelvin Probe (SKP5050) measurements were used to characterize the WF of graphene films before and after doping.

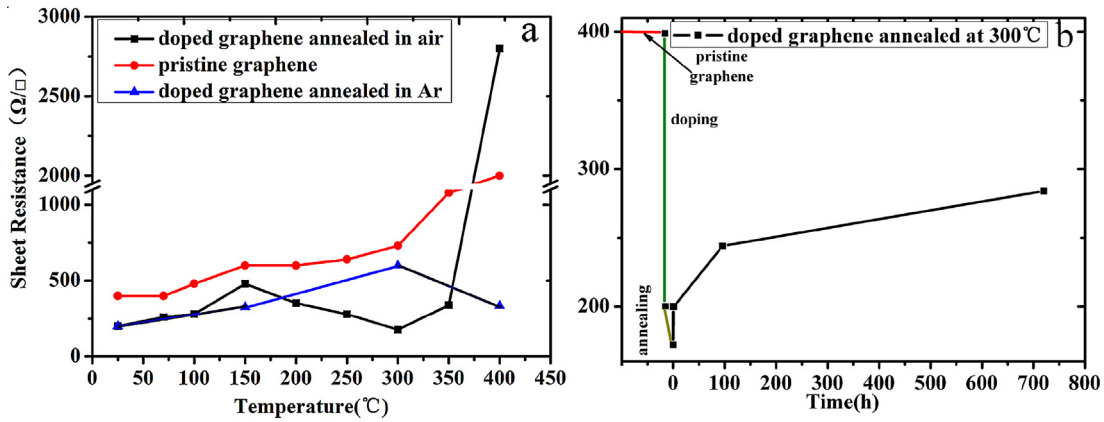

Fig. 2. (a) Sheet resistance of undoped graphene and graphene doped in air and Ar as a function of annealing temperature. The sheet resistance of pure VO_x film is not shown. (b) Sheet resistance of the doped graphene film annealed at 300 °C in air versus standing time.

3. Results and discussion

3.1. Sheet resistance, work function and transmittance of the doped graphene films

The graphene film used in this study was of 2 cm × 2 cm size, which was prepared by APCVD method. The Raman spectra of the undoped graphene are shown in Fig. 1a. The value of $I_D/I_G \approx 0.20$ confirms the low defect characteristics of the undoped graphene [22,23]. Additionally, the intensity ratio of 2D band to G band is around 1.67, which indicates that most of the graphene is of monolayer to bilayer [24]. Fig. 1b and c shows the typical process for fabricating VO_x-graphene films. The graphene TCFs consist of three layers, including quartz substrate, graphene layer and VO_x film. Firstly, the as-grown graphene TCFs were transferred onto quartz substrates. Afterwards, a thin and uniform VO_x layer was deposited by spin-coating method. Finally, the VO_x-graphene film was annealed at various temperatures for 1 h in air to further enhance the doping degree, which was the most essential step of the preparation.

Fig. 2(a) shows the sheet resistance of the undoped graphene and the doped graphene films after annealing at various temperatures in air. It can be seen that the undoped graphene exhibits a sheet resistance about 400 Ω/□, which is significantly reduced by 50% to 200 Ω/□ after doping by VO_x at room temperature (RT). It is worth noting that the sheet resistance of pure VO_x film deposited on quartz substrates is too large to be measured, while, the sheet resistance of graphene decreases sharply after depositing a layer of VO_x layer. This indicates that the doping process is highly efficient. We tried to find the optimum annealing temperature by measuring the sheet resistance. Interestingly, we find that the sheet resistance of the graphene films doped in air does not change monotonically with the temperature. The sheet resistance of doped graphene mildly increases from 200 Ω/□ to 480 Ω/□ as the temperature increases to 150 °C. While, in the region of 150–300 °C, it shows a decreasing tendency and a minimum value of 176 Ω/□ was obtained at 300 °C, corresponding to a 56% reduction compared with the initial value of 400 Ω/□ for the undoped graphene. However, the sheet resistance further increases to 2000 Ω/□ at 400 °C. We attribute this sharp increase of sheet resistance to the pronounced distortion in graphene induced by thermal annealing [25], witnessed by a similar sharp increase of bare graphene at this temperature. It can be seen that doped graphene treated at 300 °C in air shows the lowest sheet resistance, evidencing the most effective doping under this condition. In contrast, the doped graphene after Ar annealing shows higher sheet resistance. For instance, the lowest sheet resistance of Ar-annealed doped graphene is 200 Ω/□ at RT, which is 13.6% higher than the lowest value of air-treated one.

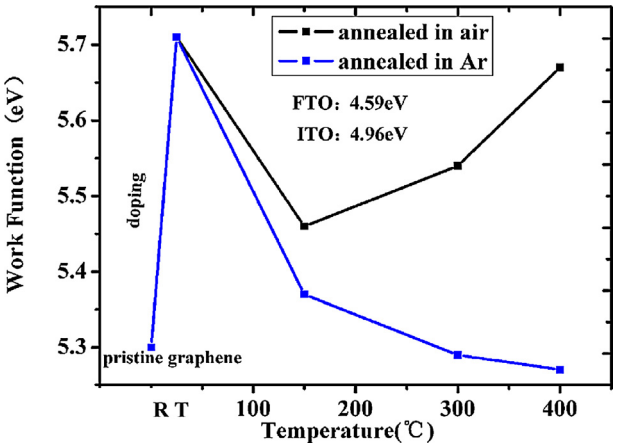

Fig. 3. Work Function of undoped graphene and graphene doped in air and Ar as a function of annealing temperature.

We compared the doping effect of VO_x for graphene with that of the commonly used dopant-HNO_3. The maximum sheet resistance reduction by VO_x doping was 56% for 300 °C air-treated ones, which is much higher than the 43% decrease caused by HNO_3 doping reported by others [26]. Our VO_x-doped graphene also demonstrates a higher stability than HNO_3-treated ones. Fig. 2(b) shows the stability of doped graphene with the lowest sheet resistance, i.e., the 300 °C air-treated one. It can be seen that the sheet resistance after 700 h standing is measured to be 280 Ω/□, a 59% increase from the initial value. This is indicative of a higher stability than some other dopants, for instance, the HNO_3 doped graphene exhibits a 90% increase of the sheet resistance after 480 h in air [27]. While in another work, the sheet resistance of $AuCl_3$ and $FeCl_3$ doped CVD graphene increases by about 80% compared with the initial value after 100 h [26].

Work function is another important parameter of the TCFs besides sheet resistance. Increasing the WF of graphene cathode can help to form Schottky contact, which can enhance the carrier injection, thereby improving the efficiency of device [28]. Fig. 3 shows the WF of doped graphene measured by KP (Kelvin Probe) analysis. After treatment, the WF of the film increases by 0.4 eV, from 5.3 eV to 5.7 eV. This clearly evidences that a p-type doping process of graphene by VO_x has occurred. As the WF of VO_x is 1.2–1.5 eV higher than that of graphene [29], a large dipole will take place at the graphene/VO_x interface for the VO_x-coated graphene

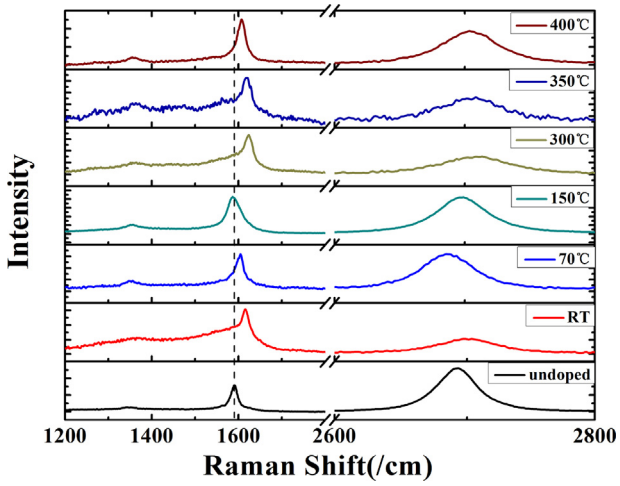

Fig. 4. Raman spectra of the undoped graphene and doped graphene annealed at different temperatures in air.

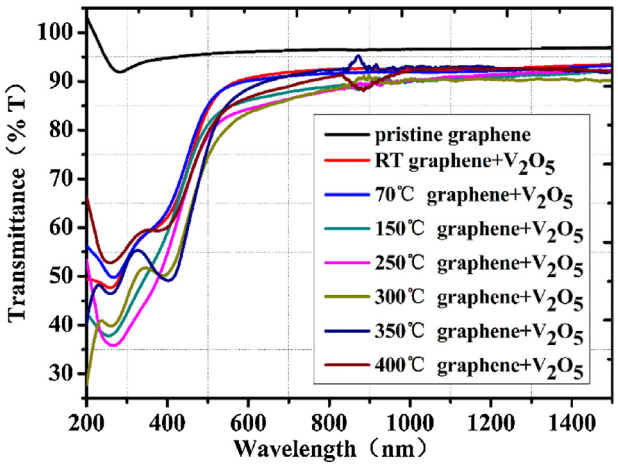

Fig. 5. Transmittance spectra of doped graphene TCFs annealed at different temperatures.

sample in our study. Some electrons will transfer from the graphene to VO_x for achieving charge neutrality at the interface, i.e., a p-type doping effect occurs for graphene. This electron transfer process causes a Fermi level alignment at the interface and leads to an increase of the WF of graphene. The WF change can also be considered as a measure of the doping degree. The more the holes injected to graphene are, the larger the WF change is caused. Based on this criterion, the doping degree is assumed to reach its minimum at 150 °C, which is consistent with that unveiled by sheet resistance.

We note that the WF of graphene measured by our work (5.3 eV) is slightly higher than the widely reported values of 4.2–4.6 eV [8,13,28–32]. This is partly ascribed to the undoped graphene exposing to the air for several days, which will lead to p-doping effect [25]. Besides, the measured WF values for ITO (4.96 eV) and fluorine-doped tin oxide(FTO) films (4.59 eV) are also 0.1–0.2 eV higher than those (4.7–4.9 eV for ITO and 4.4 eV for FTO) reported by others [2,33]. This discrepancy should be indicative of the difference in measuring conditions. Both of these two factors contribute to the slightly higher WF of the undoped graphene.

To further characterize the doping degree at various temperatures, which is reflected by sheet resistance and WF, Raman spectra measurements were further conducted due to their high sensitivity to the structural and electronic properties of graphene [34,35]. As seen in Fig. 4, The main **D, G** and **2D** features of the Raman spectra of graphene are found to arise at about 1350 cm^{-1}, 1580 cm^{-1} and 2650 cm^{-1}, respectively. The **D**-peak reflects the defects of the graphene [34]. As is illustrated in Fig. 4, the I_D/I_G ratio for doped graphene treated at different temperatures are all around 0.2–0.4, similar to that of 0.2 for undoped graphene. This result means that the VO_x doping does not cause substantial defects to the graphene, even after annealing at elevated temperatures [34,43]. This is reasonable as no lattice distortion in graphene is caused by the charge transfer doping process in our work. Similar phenomenon has also been observed in graphene doped with $AuCl_3$ [13] and thermally evaporated MoO_x [17]. The **G**-peak, which is excited by the bond stretching of all pairs of sp^2 atoms in both rings and chains, is closely related to the doping state. The **G**-peak blue shift in comparison to the undoped graphene testifies the doping from VO_x species [8], which can be attributed to the Kohn movement away from **q = 0** in Brillouin zone caused by the Femi surface change resulting from carriers transfer to graphene. The **G**-peak Raman shift of doped graphene is 27 cm^{-1} at RT, 16 cm^{-1} at 70 °C, −2 cm^{-1} at 150 °C, 35 cm^{-1} at 300 °C, 29 cm^{-1} at 350 °C and 17 cm^{-1} at 400 °C, respectively. Higher G-peak blue-shift means higher doping degree. Therefore, it can be seen that the doping degree decreases in the region of RT ~ 150 °C and 300–400 °C, whereas, it increases in the region of 150–300 °C. The doping degree exhibits a minimum at 150 °C while a maximum at 300 °C as well, which corresponds well with the trend of sheet resistance and WF. Similar to that of G-peak, 2D-peak stiffening and full width at half maximum (FWHM) can also demonstrate the p-doping degree [29]. From Fig. 4, the upshifts of 2D peak and increases of FWHM are over scales smaller than the G-peak and easily affected by environment and other factors. However, they are consistent with the trend of G-peak on the whole, which further supports that the sheet resistance and WF share the same tendency with the Raman characterization results.

As is illustrated in Fig. 5, undoped graphene shows about 96% transparency in the ultraviolet-visible-near infrared (UV–vis-NIR) range, indicating it is 1–2 layer with high transmittance, consistent with the Raman characterization results in Fig. 1a. After doping, the thickness of the coated VO_x overlayer is as thin as 10 nm, as observed from the cross sectional image of doped graphene films in Fig. S3(d). As such, the film shows 86–91% transmittance at the wavelength of 550 nm, meanwhile decreases in UV range. The excellent transmittance of doped graphene films in NIR region, which is not owned by ITO [2], is greatly promising for use in optical devices. In summary, the VO_x doping method developed by us can simultaneously reduce the sheet resistance as well as increase the WF of graphene while maintaining excellent optical transmittance.

3.2. *Evolution of VO_x in the process of heat treatment*

The doping of VO_x to graphene is significantly affected by the crystalline degree and stoichiometric ratio of VO_x species. However, no systematic study concerning the evolution of chemically obtained VO_x film upon temperature was reported. We characterized the evolution of pure VO_x film annealed at different temperatures in air by XRD analysis and the results are shown in Fig. 6. It can be seen that the as-deposited VO_x film is amorphous at RT and 150 °C. However, two obvious peaks at 20.26° and 41.26°, indexed to (001) and (113) fringes V_2O_5, respectively [JCPDS file no. 41-1426], can be found in 300 °C air-treated samples, evidencing V_2O_5 crystallization starts to occur. An interesting feature is that a small peak indexed to (600) fringe of V_3O_7 occurs at 24.45° [JCPDS file no. 27-0940], revealing the presence of oxygen vacancies. Further increase of the temperature to 400 °C witnesses narrower V_2O_5 peaks and the disappearance of V_3O_7 peak, which indicates an enhanced crystallization degree and the oxidation of low-valence vanadium species. The XRD spectra reveal an evolution process of the VO_x species with increasing temperatures, i.e.,

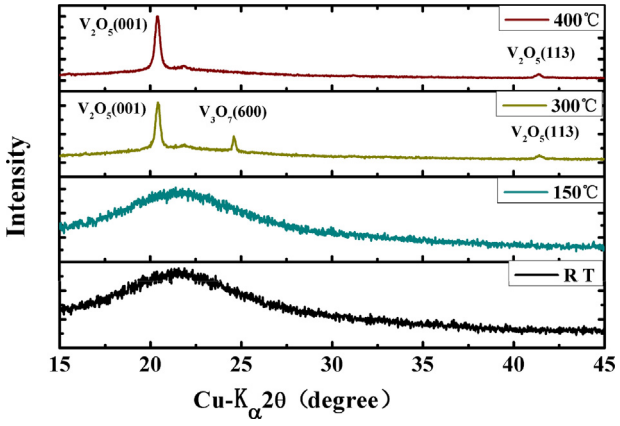

Fig. 6. XRD spectra of the doped graphene.

amorphous (RT ~ 150 °C) → amorphous V_2O_5 + crystallineV_2O_5 + O vacancies(300 °C) → crystalline V_2O_5(400 °C). As is shown in Fig. S3, this process can also be observed in the SEM micrographs. Obvious crystalline particles can only be found in Fig. S3c. We can also figure out from Fig. S3c a nearly dense VO_x coating on graphene. Therefore, it can act as effective barrier with high chemical stability, which can protect the graphene from losing the dopant in ambient air. This is why the VO_x-doped graphene can maintain a comparable stable sheet resistance with prolonged time. In contrast, the $AuCl_3$ dopant is found to form separate individual Au particles [26] and the HNO_3 dopant is volatile and unstable in ambient air [27].

XPS measurements were further conducted to better understand the composition of the doped graphene annealed at different temperatures and the spectra are shown in Fig. 7. The chemical states of V can be determined by monitoring $V_{2p}{}^{3/2}$ for V(V) at 517.16 eV, V(IV) at 515.9 eV and $V_{2p}{}^{1/2}$ for V(V) at 523.2 eV, V(IV) at 524.8 eV, respectively [36]. The ratios of V(V)/V(IV) in $V_{2p}{}^{3/2}$, calculated by the area of the peaks at RT, 150 °C and 300 °C, are 3.1, 3.3 and 7.65, which correspond to a x value of 2.378, 2.384 and 2.442, respectively. The ratio of V(V)/V(IV) becomes larger from RT to 150 °C then to 300 °C, revealing that the oxygen vacancy gets fewer as the temperature increases. However, it is notable that below 150 °C, the ratio of V(V)/V(IV) increases slower than above 150 °C. We assume the film annealed at 400 °C composed of pure V_2O_5, which is verified by the XRD spectra in Fig. 7. The X value of VO_x from RT to 400 °C falls in the range of 2.38 ~ 2.50 and the corresponding atomic oxygen percentage is 70.41–71.43%. Under these conditions, the VO_x takes the form of V_2O_5 and V_3O_7 and no other phases exist (see Fig. S1), which is consistent with the XRD results shown in Fig. 6.

In Fig. 7(d)–(f), O1 s peaks can be deconvoluted into O1 (around 530 eV for V_2O_5), O2 (at 531 eV for O in organics) and O3 (533 eV for O mainly in SiO_2) [37]. Fig. 7(e) and (d) exhibit the highest O2 intensity among Fig. 7(d)–(f), indicating the presence of large amount of O resulting from the hydrolysis reaction of vanadium precursors, which also means more O vacancies. The O2 intensity reduces for 300 °C annealed films, attributed to oxidation of vanadium species which converts the V^{4+} to V^{5+}. Therefore, the oxidation process can increase the concentration of V_2O_5, leading to an increased O1 intensity in Fig. 7f. As the detection depth of XPS is about 10 nm, the O3 signals originating from the quartz substrates for undoped graphene are sharp and strong since the graphene layer is less than 1 nm thick. In contrast, the O3 signal from VO_x-coated graphene is very weak as the VO_x layer itself is about 10 nm thick, as seen from Fig. S3(d).

Raman spectra in the region of 100–1100 cm^{-1} are illustrated in Fig. 8 to monitor the phase and oxygen vacancy evolution of VO_x species. Raman modes of V_2O_5 can be classified into internal and external vibrations with respect to the structural units. The external modes, which are located at low-frequency, can be considered as relative motions of the units, like the vanadium pentoxide layers with edge and corner sharing VO_5 square pyramids[38]. The external low-frequency Raman modes are located at about 154, 172 and 203 cm^{-1}. Below 150 °C, there are no obvious sharp peaks

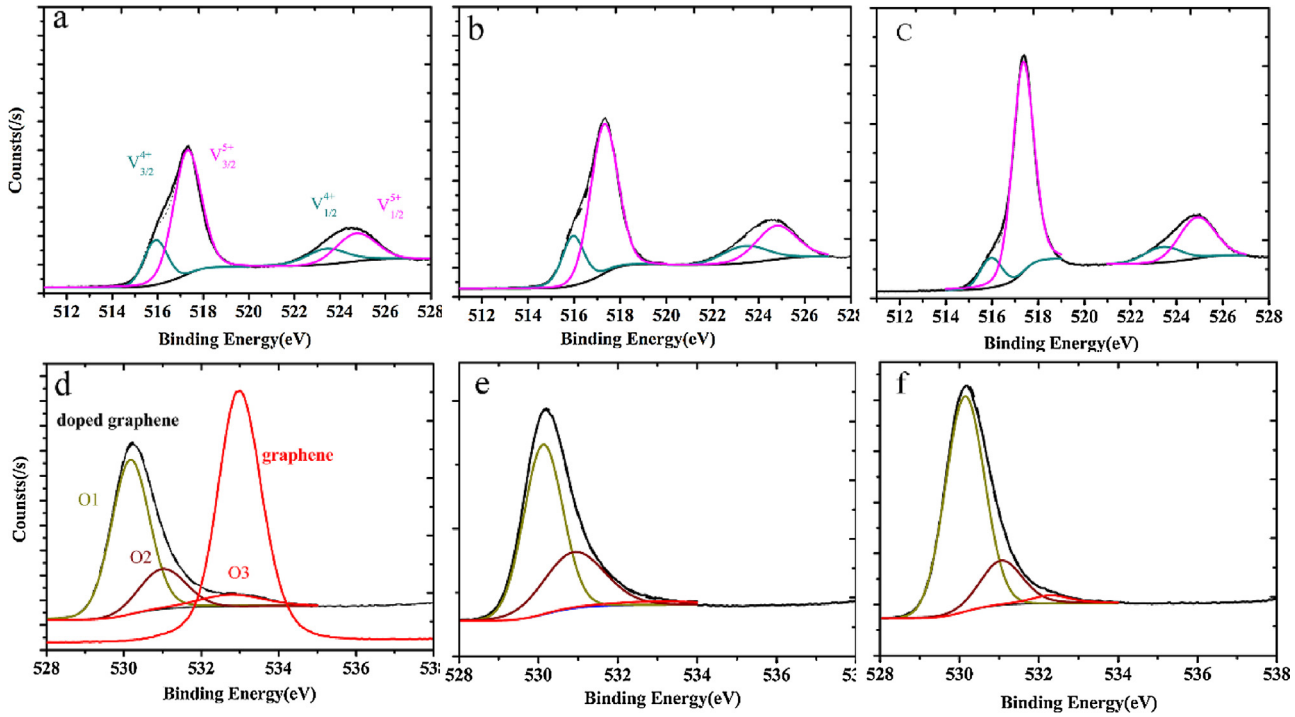

Fig. 7. XPS spectra of the V 2p peaks for doped graphene annealed at different temperatures (a. RT, b. 150 °C, c. 300 °C) and the O 1 s peaks in the undoped graphene and doped graphene. O1(VO_x), O2(C=O, etc.), O3(crystalline quartz, etc.) (d. RT, e. 150 °C, f. 300 °C). There are only O3 in undoped graphene.

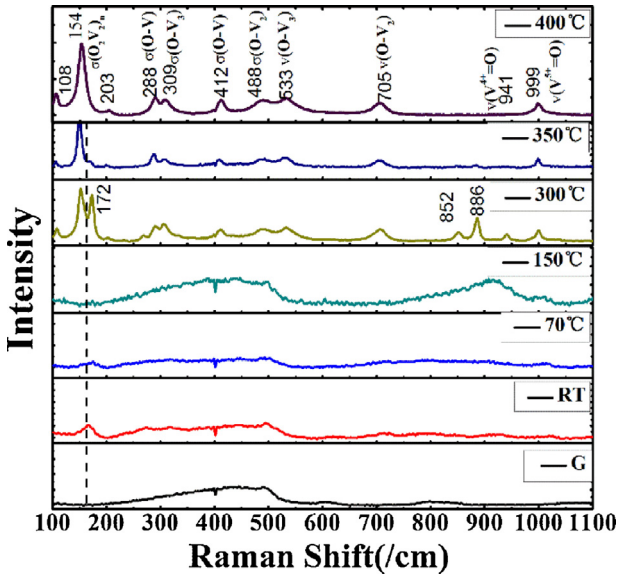

Fig. 8. Raman spectra of doped VO_x-graphene films annealed at different temperatures, as well as that of undoped graphene(G) for comparison.

except the one at 172 cm^{-1}. Considering no crystalline structure is detected in XRD spectra, it is attributed to the long-range order structure = (OV − O − OV) = [39], which is produced by the hydrolysis Reactions (1) and (2).

$$(OC_3H_7)OV(OC_3H_7)_2 + H_2O \xrightarrow{RT} (OH)OV(OC_3H_7)_2 + HOC_3H_7 \quad (1)$$

$$(OC_3H_7)OV(OC_3H_7)_2 + (OC_3H_7)OV(OC_3H_7)_2 \xrightarrow{RT} = (OV - O - OV) = + HOC_3H_7 \quad (2)$$

Except these peaks belonging to external modes, the rest belongs to the internal modes with higher frequency, which are assigned to different stretching and bending of V—O bonds [38]. The first one is the typical O-vacancy structure, which is featured by the peak V^{4+} = O at about 930 cm^{-1} for 150 °C sample. This is an evidence of the diffusion of the hydrocarbon, which extracts oxygen atoms from the vanadium pentoxide films and destroy the pristine structure [38]. Above 150 °C, the peak of V^{4+} = O shrinks, meaning that V^{4+} is gradually oxidized by O_2 to form V^{5+}. Besides the V^{4+} = O, the presence of the 852 cm^{-1} and 886 cm^{-1} peaks are indicative of crystalline VO_x with oxygen deficiencies or disorder structure [38]. Note that XPS results indicate that the V^{4+}/V^{5+} ratio monotonically decreases in the region of RT to 300 °C, the appearance of 852 and 886 cm^{-1} peaks at 300 °C only indicates a higher crystallization degree, while not a V^{4+} concentration increase. It is noteworthy that several crystalline stoichiometric V_2O_5-characteristic peaks start to appear at 300 °C, which show up at 154, 283, 288, 405, 488, 530, 705 and 999 cm^{-1}. Detail assign of these peaks is not shown here and can be referred in Ref.38. The Raman spectra results indicate an O vacancy-crystalline V_2O_5 coexisting structure in the region of 150–300 °C. The higher the temperature is, the fewer the O vacancies are, as well as more crystalline V_2O_5. Above 300 °C, the peaks corresponding to V^{4+} (886 cm^{-1}, 931 cm^{-1}) start to shrink. At 400 °C, these low-valence vanadium peaks disappear completely, as well as a remarkable increase of the intensity of V^{4+} = O peaks.

To sum up all the results in the Raman spectra, we can assert that VO_x underwent a process as follows.

RT ~ 150 °C: At RT, the vanadium(V)oxytriisopropoxide hydrolyzes to form long-range order = (OV − O − OV) = [39] in the disorder state film. As the temperature increases, the destruction of = (OV − O − OV) = structure (3), which is reflected by the disappearance of the 172 cm^{-1}, and the release of hydrocarbon leaves a portion of oxygen vacancies. O vacancy-structures crystallization under annealing result in the rising of peak of V^{4+} = O.

$$= (OV - O - OV) = \xrightarrow{150^\circ C} 2(V^{4+} = O) + O \quad (3)$$

250 °C ~ 300 °C: As the hydrocarbon in the film is exhausted, the oxidation Reaction (4) becomes increasingly dominant and the concentration of V^{4+} = O decreases gradually. The crystallization of V_2O_5 leads to coexisting structure of O vacancy-crystalline V_2O_5 at 300 °C, which is supported by Raman and XRD analysis.

$$V^{4+} = O \xrightarrow{O_2} V^{5+} = O \quad (4)$$

350–400 °C: The V^{4+} disappears gradually, O vacancies fade away and the crystallization process of V_2O_5 is completed [40,41]. From the Raman spectra, all the peaks belong to crystalline V_2O_5 structure at 400 °C.

3.3. Mechanism of doping

After spin-coating, the vanadium(V)oxytriisopropoxide was exposed to the air, which contained H_2O molecules. The hydrolysis Reactions (1) and (2) start immediately and VO_x species are thus formed [19]. Since the as-generated V^{5+} has higher WF than graphene, some holes will be injected from V^{5+} to graphene, i.e., p-type doping process occurs, as shown in (5). This process is verified by the G-peak blue-shift of Raman spectra shown in Fig. 4 and the corresponding decrease in the sheet resistance. However, as the temperature increases, the de-doping Reaction in (6) was enhanced due to diffusion of the hydrocarbon and collapse of initial VO_x structure. These two factors lead to the minimum doping degree at the temperature of 150 °C.

$$\text{Graphene} + V^{5+} \xrightarrow{RT} \text{hGraphene} + V^{4+} \quad (5)$$

$$\text{hGraphene} \xrightarrow{150^\circ C} \text{Graphene} + h \quad (6)$$

When firing temperature is over 150 °C, O vacancies get much fewer due to the filling by O_2 (4). As is well known, the WF is usually the half of the ionization energy [42]. Higher concentration of V^{5+} leads to higher WF, thereby enhancing the doping process. The doped graphene gets the utmost degree of doping at 300 °C, which is proved by the minimum sheet resistance and maximum Raman G-shift. That also explains why the doped graphene annealed in Ar atmosphere has higher sheet resistance and lower WF than in air, which can be observed by Figs. 2 a and Fig. 3. When the temperature is over 350 °C, the doping degree decreases for destroy of the graphene structure at such high temperature. The WF of doped graphene (5.65 eV), which approaches the value of crystalline V_2O_5, indicates the high crystallization degree of VO_x layer.

4. Conclusion

To conclude, we firstly used VO_x as dopant to lower the sheet resistance of undoped graphene. It is convenient and stable by using spin-coating method to deposit a thin layer of VO_x and annealing in air. The optimum heat treatment temperature was determined to be 300 °C, which results in lowest sheet resistance. The optimal VO_x-doped graphene film exhibits a 56% decrease in sheet resistance compared to undoped graphene, which is 176 Ω/□ at about 86% transmittance at 550 nm. Also the WF can be effectively increased by 0.4 eV. What is more, we firstly give a detailed research on the evolution of the VO_x species and put forward the doping mechanism. This method offers a new way for doping graphene

transparent conductive films and may shed light on expanding their application for optoelectronic purposes.

Acknowledgements

This work was supported by the National Natural Science Foundation of China(Grant No. 51272265, 61574148, 51572046, 51402340) and the State Key Laboratory for Modification of Chemical Fibers and Polymer Materials, Donghua University (Grant No. LK1517).

Appendix A. Supplementary data

Supplementary data associated with this article can be found, in the online version, at http://dx.doi.org/10.1016/j.apsusc.2016.06.086.

References

[1] K. Ellmer, Past achievements and future challenges in the development of optically transparent electrodes, Nat. Photonics 6 (2012) 809–817.
[2] J.H. Du, S.F. Pei, L.P. Ma, H.-M. Cheng, 25th anniversary article: carbon nanotube- and graphene-based transparent conductive films for optoelectronic devices, Adv. Mater. 26 (2014) 1958–1991.
[3] S. Das, P. Sudhagar, V. Verma, D. Song, E. Ito, S.Y. Lee, Y.S. Kang, W.B. Choi, Amplifying charge-transfer characteristics of graphene for triiodide reduction in dye-sensitized solar cells, Adv. Funct. Mater. 21 (2011) 3729–3736.
[4] X. Wang, L.J. Zhi, K. Mullen, Transparent, conductive graphene electrodes for dye-sensitized solar cells, Nano Lett. 8 (2008) 323–327.
[5] Y. Hao, M.S. Bharathi, L. Wang, Y. Liu, H. Chen, S. Nie, X. Wang, H. Chou, C. Tan, B. Fallahazad, H. Ramanarayan, C.W. Magnuson, E. Tutuc, B.I. Yakobson, K.F. McCarty, Y.-W. Zhang, P. Kim, J. Hone, L. Colombo, R.S. Ruoff, The role of surface oxygen in the growth of large single-crystal graphene on copper, Science 342 (2013) 720–723.
[6] R. Garg, N.K. Dutta, N.R. Choudhury, Work function engineering of graphene, Nanomaterials 4 (2014) 267–300.
[7] D.H. Kang, N. Park, J. Ko, E. Bae, W. Park, Oxygen-induced p-type doping of long individual single-walled carbon nanotube, Nanotechnology 16 (2005) 1048–1052.
[8] D. Kim, D. Lee, Y. Lee, Y.J. Duk, Work-function engineering of graphene anode by bis(trifluoromethanesulfonyl)amide doping for efficient polymer light-emitting diodes, Adv. Funct. Mater. 23 (2013) 5049–5055.
[9] H.J. Shin, W.M. Choi, D. Choi, G.H. Han, S.-M. Yoon, H.-K. Park, S.-W. Kim, Y.W. Jin, S.Y. Lee, J.M. Kim, J.-Y. Choi, Y.H. Lee, Control of electronic structure of graphene by various dopants and their effects on a nanogenerator, J. Am. Chem. Soc. 132 (2010) 15603–15609.
[10] K.K. Kim, R. Alfonso, Y. Shi, H. Park, L.-J. Li, Y.H. Lee, J. Kong, Enhancing the conductivity of transparent graphene films via doping, Nanotechnology 21 (2010) 285205.
[11] B. Guo, L. Fang, B.H. Zhang, J.R. Gong, Graphene doping: a review, Insci. J. 1 (2011) 80–89.
[12] S.M. Kim, K.K. Kim, Y.W. Jo, M.H. Park, S.J. Chae, D.L. Duong, C.W. Yang, J. Kong, Y.H. Lee, Role of anions in the $AuCl_3$-Doping of carbon nanotubes, ACS Nano 5 (2011) 1236–1242.
[13] K.C. Kwon, K.S. Choi, S.Y. Kim, Increased work function in few-layer graphene sheets via metal chloride doping, Adv. Funct. Mater. 22 (2012) 4724–4731.
[14] X.M. Li, D. Xie, H. Park, M. Zhu, T.H. Zeng, K. Wang, J. Wei, D. Wu, J. Kong, H. Zhu, Ion doping of graphene for high-efficiency heterojunction solar cells, Nanoscale 5 (2013) 1945–1948.
[15] A. Akbari-Sharbaf, S. Ezugwu, M.S. Ahmed, M.J. Cottam, G. Fanchini, Doping graphene thin films with metallic nanoparticles: experiment and theory, Carbon 95 (2015) 199–207.
[16] A. Devadoss, P. Sudhagar, S. Das, S.Y. Lee, C. Terashima, K. Nakata, A. Fujishima, W. Choi, Y.S. Kang, U. Paik, Synergistic metal–metal oxide nanoparticles supported electrocatalytic graphene for improved photoelectrochemical glucose oxidation, ACS Appl. Mater. Interfaces 6 (2014) 4864–4871.
[17] S.L. Hellstrom, M. Vosgueritchian, R.M. Stoltenberg, I. Irfan, M. Hammock, Y.B. Wang, C. Jia, X. Guo, Y. Gao, Z. Bao, Strong and stable doping of carbon nanotubes and graphene by MoO_x for transparent electrodes, Nano Lett. 12 (2012) 3574–3580.
[18] L.-Q. Mai, W. Chen, Q. Xu, J.-F. Peng, Q.-Y. Zhu, Mo doped vanadium oxide nanotubes: microstructure and electrochemistry, Chem. Phys. Lett. 382 (2003) 307–312.
[19] N. Ozer, Electrochemical properties of sol-gel deposited vanadium pentoxide films, Thin Solid Films 305 (1997) 80–87.
[20] M.B. Sahana, C. Sudakar, C. Thapa, G. Lawes, V.M. Naik, R.J. Baird, G.W. Auner, R. Naik, K.R. Padmanabhan, Electrochemical properties of V_2O_5 thin films deposited by spin coating, Mater. Sci. Eng. B: Adv. 143 (2007) 42–50.
[21] K. Zilberberg, S. Trost, J. Meyer, A. Kahn, A. Behrendt, D. Lützenkirchen-Hecht, R. Frahm, T. Riedl, Inverted organic solar cells with sol–gel processed high work-function vanadium oxide hole-extraction layers, Adv. Funct. Mater. 21 (2011) 4776–4783.
[22] D. Teweldebrhan, A.A. Balandin, Modification of graphene properties due to electron-beam irradiation, Appl. Phys. Lett. 94 (2009) 013101.
[23] J.-Y. Hwang, C.-C. Kuo, L.-C. Chen, K.-H. Chen, Correlating defect density with carrier mobility in large-scaled graphene films: Raman spectral signatures for the estimation of defect density, Nanotechnology 21 (2010) 465705.
[24] Y. Wu, B. Wang, Y. Ma, Y. Huang, N. Li, F. Zhang, Y. Chen, Efficient and large-scale synthesis of few-layered graphene using an arc-discharge method and conductivity studies of the resulting films, Nano Res. 3 (2010) 661–669.
[25] S. Ryu, L. Liu, S. Berciaud, Y.-H. Yu, H.T. Liu, P. Kim, G.W. Flynn, L.E. Brus, Atmospheric oxygen binding and hole doping in deformed graphene on a SiO_2 substrate, Nano Lett. 10 (2010) 4944–4951.
[26] Y. Song, W. Fang, A.L. Hsu, J. Kong, Iron (III) chloride doping of CVD graphene, Nanotechnology 25 (2014) 395701.
[27] C.W. Jang, J.M. Kim, J.H. Kim, D.H. Shin, S. Kim, S.-H. Choi, Degradation reduction and stability enhancement of p-type graphene by $RhCl_3$ doping, J. Alloys Compd. 621 (2015) 1–6.
[28] C.K. Kwon, K.S. Choi, B.J. Kim, J.-L. Lee, S.Y. Kim, Work-function decrease of graphene sheet using alkali metal carbonates, J. Phys. Chem. C 116 (2012) 26586–26591.
[29] I. Hancox, L.A. Rochford, D. Clare, M. Walker, J.J. Mudd, P. Sullivan, S. Schumann, C.F. McConville, T.S. Jones, Optimization of a high work function solution processed vanadium oxide hole-extracting layer for small molecule and polymer organic photovoltaic cells, J. Phys. Chem. C 117 (2013) 49–57.
[30] K.W. Kim, W. Song, M.W. Jung, M.-A. Kang, S.Y. Kwon, S. Myung, J. Lim, S.S. Lee, K.-S. An, Au doping effect on chemically-exfoliated graphene and graphene grown via chemical vapor deposition, Carbon 82 (2015) 96–102.
[31] K.W. Kim, W. Song, M.W. Jung, M.-A. Kang, S.Y. Kwon, S. Myung, J. Lim, S.S. Lee, K.-S. An, Au doping effect on chemically-exfoliated graphene and graphene grown via chemical vapor deposition, Carbon 82 (2015) 96–102.
[32] I.E. Wachs, Catalysis science of supported vanadium oxide catalysts, Dalton Trans. 42 (2013) 11762–11769.
[33] M.G. Helander, M.T. Greiner, Z.B. Wang, W.M. Tang, Z.H. Lu, Work function of fluorine doped tin oxide, J. Vac. Sci. Technol. A 29 (2011) 011019.
[34] A.C. Ferrari, Raman spectroscopy of graphene and graphite:disorder, electron–phonon coupling, doping and nonadiabatic effects, Solid State Commun. 143 (2007) 47–57.
[35] Y. Hao, L. Wang, Y. Liu, H. Chen, X. Wang, C. Tan, S. Nie, J.W. Suk, T. Jiang, T. Liang, J. Xiao, W. Ye, C.R. Dean, B.I. Yakobson, K.F. McCarty, P. Kim, J. Hone, L. Colombo, R.S. Ruoff, Oxygen-activated growth and bandgap tunability of large single-crystal bilayer graphene, Nat. Nanotecnol. (2016), advance online publication.
[36] M.C. Biesinger, L.W.M. Lau, A.R. Gerson, R.S.C. Smart, Resolving surface chemical states in XPS analysis of first row transition metals, oxides and hydroxides: Sc, Ti, V, Cu and Zn, Appl. Surf. Sci. 257 (2010) 887–898.
[37] G. Sadanandam, K. Lalitha, V.D. Kumari, M.V. Shankar, M. Subrahmanyam, Cobalt doped TiO_2: a stable and efficient photocatalyst for continuous hydrogen production from glycerol: water mixtures under solar light irradiation, Int. J. Hydrogen Energy 38 (2013) 9655–9664.
[38] M.B. Sahana, C. Sudakar, C. Thapa, G. Lawes, V.M. Naik, R.J. Baird, G.W. Auner, R. Naik, K.R. Padmanabhan, Electrochemical properties of V_2O_5 thin films deposited by spin coating, Mater. Sci. Eng. B 143 (2007) 42–50.
[39] I.E. Wachs, Catalysis science of supported vanadium oxide catalysts, Dalton Trans. 42 (2013) 11762–11769.
[40] J. Livage, Vanadium pentoxide gels, Chem. Mater. 3 (1991) 578–593.
[41] J. Haber, M. Witko, R. Tokarz, Vanadium pentoxide I. Structures and properties, Appl. Catal. A: Gen. 157 (1997) 3–22.
[42] D.J.D. Moet, P. de Bruyn, P.W.M. Blom, High work function transparent middle electrode for organic tandem solar cells, Appl. Phys. Lett. 96 (2010) 153504.
[43] M. Bruna, A.K. Ott, M. Ijäs, D. Yoon, U. Sassi, A.C. Ferrari, Doping dependence of the Raman spectrum of defected graphene, ACS Nano. 8 (2014) 7432–7441.